Exciton and polariton dispersion curves of $In_xGa_{1-x}As/GaAs(001)$ superlattice quantum wells: Model calculation

N. Tomassini,* D. Schiumarini, L. Pilozzi, and A. D'Andrea
Istituto dei Sistemi Complessi, CNR, Casella Postale 10, Monterotondo Stazione, Rome I-00016, Italy
(Received 22 June 2006; revised manuscript received 2 November 2006; published 14 February 2007)

Wannier exciton dispersion curves of $In_xGa_{1-x}As/GaAs(001)$ quantum well superlattice are obtained by computing exciton energies, for different $\boldsymbol{K}$ points in the corresponding Brillouin zone, using a variational exciton envelope function model. The effective mass and the spatial dispersion of the exciton show strong variations depending on energy bands and $\boldsymbol{K}$ points. Polariton dispersion curves are computed in the semiclassical framework by using a nonlocal exciton susceptibility and solving self-consistently the Schrödinger-Maxell equations. Photon dispersion curves of the one-dimensional photonic crystal, resulting from the periodicity of the dielectric constant in the superlattice, are also computed and reported in comparison with exciton and polariton bands. In order to mimic mesoscopic uniaxial photonic crystals, the versatility of $In_xGa_{1-x}As/GaAs(001)$ superlattice is highlighted by selected numerical examples.

DOI: 10.1103/PhysRevB.75.085317 PACS number(s): 78.67.De, 78.67.Pt, 71.35.−y, 71.36.+c

I. INTRODUCTION

The Wannier exciton-polariton, propagating in a quantum well superlattice (SLQW), has attracted a lot of interest since the beginning of optical response study in mesoscopic structures.[1–9] In fact, this radiation-matter interaction allows the optical tailoring of the system to be performed by taking into account the following physical parameters: (i) the exciton energy, (ii) its envelope function, both affected by quantum and dielectric confinements, and (iii) the spatial confinement of the electromagnetic field. Besides, the SLQW has very recently[10,11] been considered a paradigmatic model since it can mimic different interesting optical systems, namely, (i) mesoscopic uniaxial semiconductor crystal[12,13] with respect to the Wannier exciton energy bands, (ii) one-dimensional (1D) photonic crystals with respect to the background dielectric constant modulation, and finally, (iii) 1D resonant photonic crystals (or polaritonic crystals) in the case of photon energies close to the Wannier exciton transition.[10,11]

It is well known that the biaxial misfit strain in lattice-mismatched [001] oriented heterostructures deforms the isometric zinc blende [$In_xGa_{1-x}As/GaAs(001)$] structure into tetragonal. Therefore, the strain shifts conduction- and valence-band levels and completely removes the degeneracy at the Γ point of the *p*-like valence-band states already split by the spin-orbit interaction.[14–19] Moreover, the effective valence-band masses become anisotropic, due to the cylindrical symmetry induced by the biaxial strain, and assume different values of the parallel and perpendicular components with respect to the superlattice axis.[17] The energy splitting at the Γ point of the valence band allows the formation of different valence-conduction transitions that correspond to three different kinds of exciton: heavy-hole (hh-e), light-hole (lh-e), and split-off (so-e). These three excitons show a different dynamics due to their effective masses and finite confining potentials, and their interaction gives appreciable contributions to the exciton energy values.

Electrons and holes, propagating in heteropolar solids, interact with the ion cores of the crystal and produce local lattice deformations that modify the screening of the electron-hole Coulomb interaction. A remarkable effect of this so-called polaron interaction[20] is the increase of the charge-carrier effective masses as a consequence of the ionic field contribution to their motion. Finally, excitons penetrate into the finite potential barriers of the quantum well and feel a dielectric mismatch that also modifies the screening of the electron-hole Coulomb interaction. This effect, commonly called "dielectric confinement,"[21] increases by increasing the dielectric mismatch and, in the present calculation, it is modeled by the image potential formalism.

It should be noted that all these physical effects influence the binding energies and the oscillator strength of the confined exciton, and, therefore, they will be embodied on an equal footing into the present theoretical model.

The aim of the present work is twofold: (i) to present a variational model for studying periodic semiconductor heterostructures by means of calculations of Wannier exciton energies and binding energies in $In_xGa_{1-x}As/GaAs(001)$ SLQW, and (ii) to study photon and polariton dispersion curves by self-consistent Maxwell-Schrödinger calculations in the semiclassical framework and in the effective-mass approximation.

The Schrödinger-Maxwell semiclassical framework adopted is known to be a rather general theoretical scheme for computing the optical response of mesoscopic systems when the exciton nonlocal dielectric function is considered.[4,9]

In conclusion, the main physical properties embodied in the present model are (i) interaction among valence bands split by the strain, (ii) anisotropic effective band masses, (iii) charge image potential, (iv) polaronic contributions to the Coulomb potential, and (v) nonlocal polarization (spatial dispersion) of Wannier exciton.

The theoretical framework used to calculate excitons and polaritons in SLQW is presented in Sec. II, while results and discussions are reported in Sec. III. Section IV is devoted to a brief summary and conclusions.

II. MODEL CALCULATION

A. Excitons in a SLQW

The theoretical study of excitons, confined in a SLQW, involves the solution of Schrödinger equation in periodic heterostructures where the confining potentials, the dielectric function, and the effective masses show the full translational symmetry of the lattice. For this purpose, periodic heterostructures constituted of layers of $In_xGa_{1-x}As$ (x=0.185), sandwiched between layers of GaAs [001] oriented, have been chosen as model for calculations.

The Wannier exciton is computed in the effective-mass approximation by an accurate variational model well suited to describe energy states and optical response of the system.

The total Hamiltonian for heavy-hole, light-hole, and split-off excitons can be written down as a 3×3 block matrix whose elements are $H_{h',h}=\langle\Psi_{e\text{-}h'}|H|\Psi_{e\text{-}h}\rangle$ with e =electron, h=hole, and Ψ represents an excitonic state:

$$H_{e\text{-}h}=\begin{pmatrix} H_{\mathrm{hh,hh}} & H_{\mathrm{hh,lh}} & H_{\mathrm{hh,so}} \\ H_{\mathrm{lh,hh}} & H_{\mathrm{lh,lh}} & H_{\mathrm{lh;so}} \\ H_{\mathrm{so,hh}} & H_{\mathrm{so,lh}} & H_{\mathrm{so,so}} \end{pmatrix}. \tag{1}$$

In the calculations, the negligible interactions of the heavy-hole exciton with light-hole and split-off excitions have been disregarded.[15,22,23]

The general expression, in cylindrical coordinates, for the diagonal elements of the Hamiltonian operator is

$$\begin{aligned} H_{e\text{-}h}=&-\frac{1}{2\mu_{x,y}}\nabla_\rho^2-\frac{1}{2}\frac{\partial}{\partial z_e}\frac{1}{m_e(z_e)}\frac{\partial}{\partial z_e}-\frac{1}{2}\frac{\partial}{\partial z_h}\frac{1}{m_h(z_h)}\frac{\partial}{\partial z_h}\\ &+V_{eff}(r)-\alpha_e\omega_{\mathrm{LO}}-\alpha_h\omega_{\mathrm{LO}}+V_{im}(r)+V_e^o(z_e)+V_h^o(z_h)\\ &+E_g^{e\text{-}h}, \end{aligned} \tag{2}$$

while the z component of the kinetic operator of the off-diagonal lh-so element is[17,18]

$$T_{\mathrm{lh,so}}=-\frac{1}{\sqrt{2}}\frac{\partial}{\partial z}\left[\frac{1}{m_{\mathrm{so}}(z)}-\frac{1}{m_h(z)}\right]\frac{\partial}{\partial z}. \tag{3}$$

The z axis is oriented along the [001] direction and $r=\sqrt{(z_e-z_h)^2+\rho^2}$. $V_e^o(z_e)$ and $V_h^o(z_h)$ are the confining potentials for electrons and holes, respectively, while m_i ($i=e,h$) is the position-dependent effective mass renormalized by the interaction with longitudinal optical phonons, as described below. The z and in-plane (x,y) components of the effective band-mass tensor, split by the cylindrical symmetry, are related to the well-known Kohn-Luttinger parameters[24,25] γ_1 and γ_2 as given in the following equations:

$$m_{\mathrm{hh}}^*(z)=\frac{1}{\gamma_1-2\gamma_2},\quad m_{\mathrm{lh}}^*(z)=\frac{1}{\gamma_1+2\gamma_2},$$

$$m_{\mathrm{so}}^*(z)=m_{\mathrm{so}}^*(x,y)=\frac{1}{\gamma_1},$$

$$m_{\mathrm{hh}}^*(x,y)=\frac{1}{\gamma_1+\gamma_2},\quad m_{\mathrm{lh}}^*(x,y)=\frac{1}{\gamma_1-\gamma_2}. \tag{4}$$

The polaron contribution has been derived from the model proposed by Bajaj and co-workers;[26,27] in accordance with this model, both the z and in-plane masses scale as $m_i=m_i^*[(12+\alpha_i)/(12-\alpha_i)]$ ($i=e,h$), where the dimensionless coupling parameter α_i, measuring the strength of the interaction between electrons (holes) and lattice longitudinal optical phonons, is

$$\alpha_i=\frac{1}{2\bar{\varepsilon}}\sqrt{\frac{2m_i^*}{\omega_{\mathrm{LO}}}}\quad\text{with}\quad\frac{1}{\bar{\varepsilon}}=\left(\frac{1}{\varepsilon_\infty}-\frac{1}{\varepsilon_B}\right),$$

ε_B and ε_∞ are the static and the high-frequency dielectric constants, respectively, and ω_{LO} is the longitudinal optical phonon frequency.

The effective potential $V_{eff}(r)$ comes from the Coulomb electron-hole interaction screened by the LO phonons. In the present calculation, we have adopted as effective potential the functional given in Refs. 26 and 27, namely,

$$\begin{aligned} V_{eff}(r)=&-\frac{1}{\varepsilon_B r}-\frac{1}{2\bar{\varepsilon}r}(e^{-\beta_e r}+e^{-\beta_h r})+\frac{1}{2\bar{\varepsilon}}C_e e^{-\beta_e r}\\ &+\frac{1}{2\bar{\varepsilon}}C_h e^{-\beta_h r}, \end{aligned}$$

$$\text{where } C_i=\frac{\beta_i}{[1+\alpha_i/4(1+\alpha_i/12)^2](1+\alpha_i/12)}\quad\text{with } i=e,h, \tag{5}$$

$\alpha_e\omega_{\mathrm{LO}}$ and $\alpha_h\omega_{\mathrm{LO}}$ are the polaron self-energies for electrons and holes, respectively.

The dielectric confinement is embodied into the Hamiltonian by the image potential V_{im} given in Refs. 28 and 29 and it will not be discussed further here.

All the calculations have been performed for T=9 K, and the adopted values of the physical parameters are those of the pure materials,[30,31] namely, γ_1=6.85, γ_2=2.10, ε_B=12.53, and ε_∞=10.90 for GaAs, and γ_1=19.67, γ_2=8.27, ε_B =14.60, and ε_∞=12.25 for InAs, from which the corresponding parameters of the alloy material are obtained by using a linear interpolation scheme, as reported in Refs. 18 and 31.

The energy band gaps of the heavy, light, and split-off holes are obtained by computing the shift of the different band states produced by the misfit strain of the heterostructure with respect to the band-gap energy of the unstrained $In_xGa_{1-x}As$ alloy, as reported in Ref. 18. This latter energy gap is computed as function of the temperature and of alloy composition x by the following nonlinear interpolation formula:[32]

$$E_g(x,T)=E_g(0,0)+ax+bx^2-(c+dx)\frac{T^2}{T+(ex+f)},$$

where $E_g(0,0)$=1.5192 eV, a=−1.597 eV, b=0.5 eV, c =5.408×10^{-5} eV/K, d=-9.4×10^{-4} eV/K, e=183 K, and f=204 K.

The variational exciton envelope functions are expanded in products of electron and hole subbands, $u_i^e(z_e)u_j^h(z_h)$ combined with optimized hydrogenic $1S$ radial wave functions: $\phi_{ij}(r)=\exp(-r/\lambda_{ij})$. The quantity λ_{ij} is also chosen as variational parameter and optimized for each basis function.

In principle, the SLQW subband functions must fulfill the condition of continuity, at each interface of the heterostructure, together with the periodicity condition at the boundaries of the SLQW unit cell. Moreover, as in any periodic potential problem, the overall solution must be of the Bloch form. All these conditions can be satisfied by using, as subbands, Bloch-type functions computed, for each heterolayer constituting the SLQW cell, as solutions of the Hamiltonian of Eq. (2) in which all the electron-hole interaction contributions are wiped out:

$$u_j(z;K) = [A_j e^{ik_j z} + B_j e^{-ik_j z}]e^{-i\mathbf{K}\mathbf{z}}. \tag{6}$$

$\boldsymbol{K}$ defines a point inside the 1D Brillouin zone (BZ) of the SLQW, and

$$k_j = \sqrt{2m_j(E - V_j^o + \alpha_j\omega_{\mathrm{LO}})}, \tag{7}$$

where m_j is the z component of the electron (hole) mass.

The phase amplitude values A_j and B_j are obtained, for each j layer of the elementary cell, by imposing the continuity of the current density at each j interface together with the periodicity condition. Their values, in two adjacent heterolayers (j and $j+1$) of the heterostructure, are related by the transfer matrix M_j computed at the j interface:

$$\begin{pmatrix} A_{j+1} \\ B_{j+1} \end{pmatrix} = M_J \begin{pmatrix} A_j \\ B_j \end{pmatrix} \tag{8}$$

with

$$M_j = \frac{m_{j+1}^2}{4k_{j+1}^2} \begin{pmatrix} \dfrac{m_j k_{j+1} + m_{j+1}k_j}{m_j m_{j+1}} e^{-i(k_{j+1}-k_j)z_j} & \dfrac{m_j k_{j+1} - m_{j+1}k_j}{m_j m_{j+1}} e^{-i(k_{j+1}+k_j)z_j} \\ \dfrac{m_j k_{j+1} - m_{j+1}k_j}{m_j m_{j+1}} e^{i(k_{j+1}+k_j)z_j} & \dfrac{m_j k_{j+1} + m_{j+1}k_j}{m_j m_{j+1}} e^{i(k_{j+1}-k_j)z_j} \end{pmatrix}. \tag{9}$$

In a SLQW unit cell, embodying n heterolayers, the continuity condition gives

$$\begin{pmatrix} A_{n+1} \\ B_{n+1} \end{pmatrix} = M_n \cdots M_2 M_1 \begin{pmatrix} A_1 \\ B_1 \end{pmatrix} = M \begin{pmatrix} A_1 \\ B_1 \end{pmatrix}, \tag{10}$$

while the periodicity condition is given by the following matrix equation:

$$\begin{pmatrix} A_{n+1} \\ B_{n+1} \end{pmatrix} = P \begin{pmatrix} A_1 \\ B_1 \end{pmatrix} \tag{11}$$

with P periodicity matrix:

$$P = e^{-iKt} \begin{pmatrix} e^{ik_1 t} & 0 \\ 0 & e^{-ik_1 t} \end{pmatrix}, \tag{12}$$

where $\boldsymbol{t}$ is the translation vector of the 1D cell.

From Eqs. (10) and (11) we obtain the homogeneous equation

$$(M - P)\begin{pmatrix} A_1 \\ B_1 \end{pmatrix} = \begin{pmatrix} 0 \\ 0 \end{pmatrix} \tag{13}$$

that can be solved as a secular equation problem,

$$|M - P| = |M| + |P| - (M_{11}P_{22} + M_{22}P_{11}) = 0, \tag{14}$$

in order to obtain the subband energy states and the coefficients A_j and B_j for all the j layers of the SLQW cell.

Wannier exciton wave functions are given as a variational expansion according to

$$\Psi_n(z_e, z_h, \rho; K) = \sum_{i,j} C_{ij,n} u_i^e(z_e;K) u_j^h(z_h;K) \phi_{ij}(z_e, z_h, \rho; \lambda_{ij}), \tag{15}$$

and the exciton states are computed along the line of Refs. 9 and 33. Moreover, for wave vectors $\boldsymbol{K}$ in the first BZ, each exciton state defines a band of energy and, therefore, the dispersion curves of the exciton states in SLQW can be computed.

B. Polaritons in SLQW

Now, let us consider the polariton dispersion curves for a SLQW of $Ga_{1-x}In_xAs/GaAs(001)$. The nonlocal linear polarization vector is given by

$$4\pi \boldsymbol{P}(z;\omega) = \sum_n S_n(\omega)\Psi_n^*(z;K) \int_L \Psi_n(z';K)\boldsymbol{E}(z';\omega,K), \tag{16}$$

where $z_e=z_h=z$. The Maxwell equation for an electromagnetic wave at normal incidence and for each point $\boldsymbol{K}$ of the first BZ is (in a.u.)

$$\frac{d^2\boldsymbol{E}(z;\omega,K)}{dz^2} = -\frac{\omega^2}{c^2}\varepsilon_B(z)\boldsymbol{E}(z;\omega,K) - \frac{\omega^2}{c^2}\sum_n S_n(\omega)\Psi_n^*(z;K) \times \int_L dz'\Psi_n(z';K)\boldsymbol{E}(z';\omega,K), \tag{17}$$

where $\varepsilon_B(z)$ is the background dielectric constant modulation.

The integration on $z\prime$ is performed on the volume L of the 1D unit cell of the SLQW, and the summation is over the excitonic states Ψ_n with energy ω_n. The quantities $S_n(\omega)$ are

$$S_n(\omega) = \frac{S_o(\omega)}{\omega_n - \omega - i\gamma} \tag{18}$$

with

$$S_o(\omega) = 2\pi g\frac{\omega_K}{\omega^2}, \tag{19}$$

where ω_K is the Kane energy of the interband transition, g is the multiplicity of the exciton state ($g=3/4$ and $g=1/4$ for the hh-e and lh-e excitons, respectively),[19] and γ is the nonradiative homogeneous broadening that, for very low temperatures, is essentially due to the exciton acoustic-phonon scattering. In the present calculation, it is taken as a constant value.

The formal solution of Eq. (17) is performed by using the Green function method[34] along the line of Refs. 9 and 33 and the resulting electric field in each j layer (L_j) is

$$E_j(z;\omega,K) = A_j\alpha_j(z;\omega,K) + B_j\beta_j(z;\omega,K), \tag{20}$$

where

$$\alpha_j = e^{iq_jz} - \sum_m \frac{\omega^2}{c^2}\int_{L_j} dz'\ g_j(z,z')\Psi_m(z';K)\sum_n D_{mn}^{-1}(\omega,K) \times \int_{L_J} dz\ \Psi_n^*(z,K)e^{iq_jz}, \tag{21}$$

$$\beta_j = e^{-iq_jz} - \sum_m \frac{\omega^2}{c^2}\int_{L_j} dz'\ g_j(z,z')\Psi_m(z';K)\sum_n D_{mn}^{-1}(\omega,K) \times \int_{L_J} dz\ \Psi_n^*(z,K)e^{-iq_jz}, \tag{22}$$

with $q_j=(\omega/c)\sqrt{\varepsilon_B(z_j)}$,

$$g_j(z,z') = \frac{\Theta(z-z')e^{iq_j(z-z')} + \Theta(z'-z)e^{iq_j(z'-z)}}{i2q_j} \tag{23}$$

is the Green function, and $D_{mn}^{-1}(\omega,K)$ are the elements of the inverse of the polaritonic matrix D with

$$D_{mm} = S_o^{-1}\left[\omega_m + S_o\frac{\omega^2}{c^2} \times \int_{L_j} dz\ \Psi_m^*(z,K)\int_{L_j} dz'\ \Psi_m(z',K)g(z,z') - \omega - i\gamma\right], \tag{24}$$

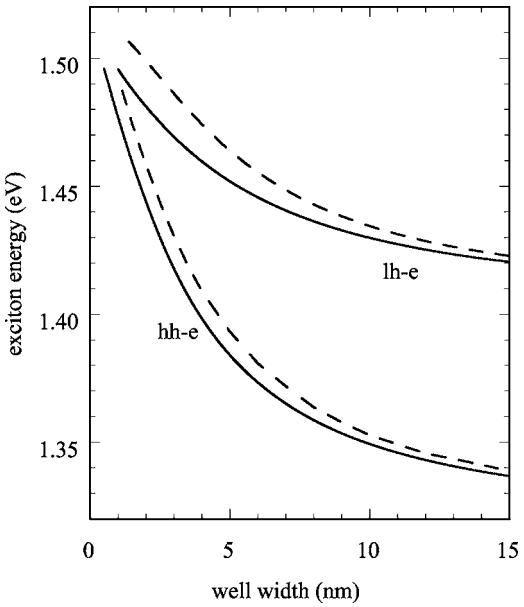

FIG. 1. Energies computed for hh-e and lh-e in $In_xGa_{1-x}As/GaAs(001)$ SLQW (solid lines) and in a single QW (dashed lines).

$$D_{mn} = \frac{\omega^2}{c^2}\int_{L_j} dz\ \Psi_m^*(z,K)\int_{L_j} dz'\ \Psi_n(z',K)g(z,z') \tag{25}$$

the diagonal and off diagonal matrix elements, respectively.

The coefficients A_j and B_j of Eq. (20) are obtained, for each j layer of the SLQW cell, by imposing the condition of continuity of the in-plane electric field, at each interface, and the periodicity at the boundaries of the unit cell. These conditions give rise to a secular equation for the electric field $\boldsymbol{E}$, formally analogous to that previously introduced for the calculation of the subband functions [see Eqs. (10)–(14)], from

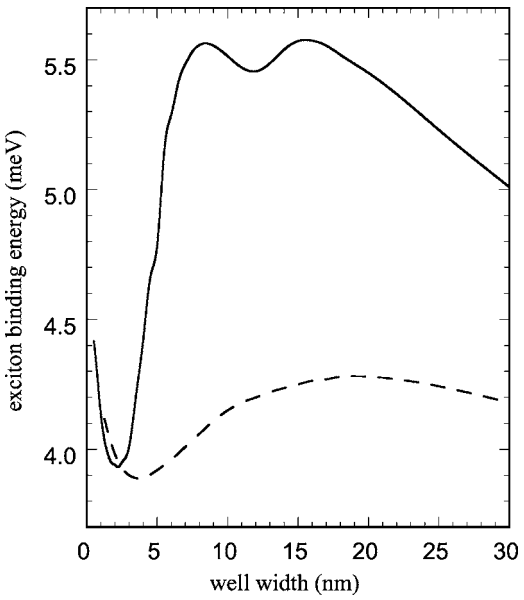

FIG. 2. Exciton binding energies computed for hh-e (solid line) and lh-e (dashed line) in $In_xGa_{1-x}As/GaAs(001)$ SLQW.

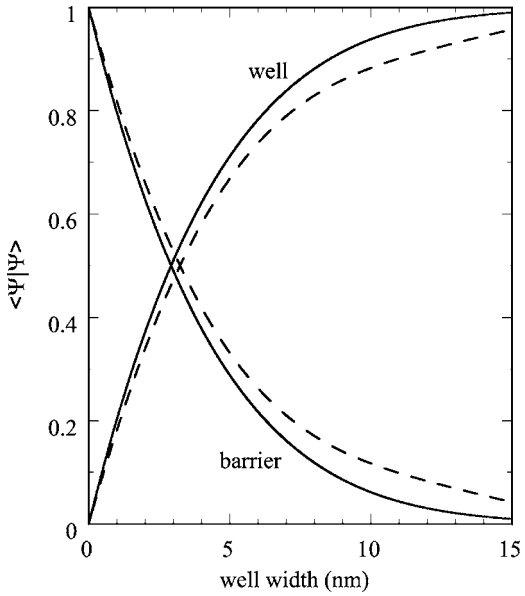

FIG. 3. Exciton localization probability of hh-e (solid line) and lh-e (dashed line) in the well and in the barrier computed as a function of well width in SLQW.

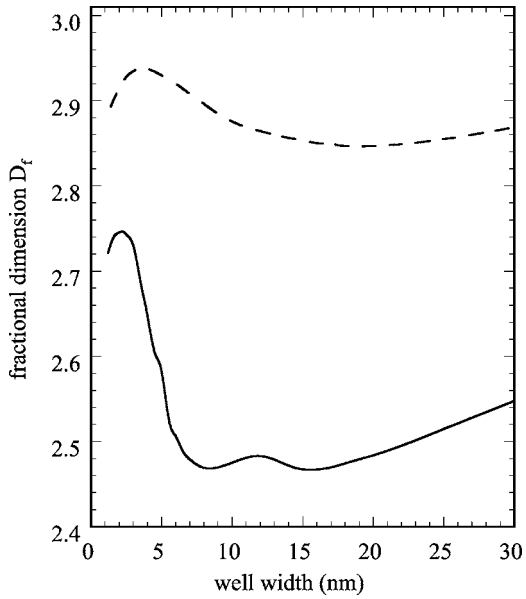

FIG. 4. Fractional space dimension computed for hh-e (full line) and lh-e (dashed line) as a function of the well width.

which the polariton energies ω are obtained as a function of the $\boldsymbol{K}$ wave vectors.

Moreover, taking into account only the background dielectric function modulation [$S_o=0$ in Eq. (17)], the photonic dispersion curves of the superlattice can also be computed.

Finally, the normal incidence reflectivity spectrum can be obtained by computing the solutions of Eq. (20) as a function of ω for a fixed $\boldsymbol{K}$ value.

It should be emphasized that the present model calculation, based on a generally accepted semiclassical framework where Schrödinger and Maxwell equations are self-consistently solved,[4,9] avoids the use of *ad hoc* assumptions such as the so-called additional boundary conditions,[4,6,35] and, indeed, the only fitting parameter embodied in the theory is the nonradiative homogeneous broadening γ.

III. RESULTS AND DISCUSSION

A. Excitons in SLQW

Let us consider an $In_xGa_{1-x}As/GaAs(001)$ SLQW with indium concentration $x=0.185$. The exciton transition energies of the lowest hh-e and lh-e exciton levels, as a function of well width, in the case of barrier thickness $L_b=5$ nm, are shown in Fig. 1. The hh-e and lh-e exciton energies, computed for a single quantum well with $L_b=200$ nm, are also reported in the same figure for the sake of comparison. It should be noticed that all the curves show the same behavior as a function of the well width, but the energy of exciton in SLQW is systematically smaller than that in the single quantum well system. This property is due to the lower confinement experienced by the exciton propagating in the SLQW. The maximum energy difference, of about 20 meV for both the excitons, is observed for the thinnest well widths (of about 1 nm).

The exciton binding energies of the lowest hh-e and lh-e exciton levels, computed at Γ point as a function of well width, are shown in Fig. 2. The behavior of the hh-e binding energy is surprising if compared with the binding energy in a single QW where only a maximum, corresponding to the so-called pseudo two-dimensional (2D) to three-dimensional (3D) transition, is present.[18] At variance with this well-known case, the calculations in SLQW clearly show two different maximum values at about 8 and 15.5 nm, respectively.

In order to explain this interesting result, let us go back to Fig. 1 where, for large value of well width, the exciton energy in the superlattice is close to that confined in the single quantum well. Now, by decreasing the well thickness, the binding energy increases toward the two-dimensional limit [$E_b(2D)=4E_b(3D)$] of $In_xGa_{1-x}As$ quantum well, until it reaches the maximum confinement energy obtained for the well width value of about 15.5 nm. For smaller well widths, the exciton delocalizes in the barriers and restores its three-dimensional behavior, and the exciton binding energy undergoes a minimum value. Finally, for very thin quantum wells, exciton delocalizes throughout the SLQW and its binding energy is due to the interplay between confinement and periodicity effects. In this latter case, the maximum confinement in the SLQW is observed at about 8 nm, while the minimum is close to 2.5 nm, where equal probabilities are obtained for Wannier exciton localized inside the wells or in the barriers as is clearly shown in Fig. 3.

Different from the heavy-hole exciton behavior, the light-hole exciton binding energy, in the SLQW, shows a single but very broad maximum at about 19 nm; this is because, as in the case of the single QW,[18,32] the SLQW lh-e exciton experiences a weak confinement. It should be noted that the polaron interaction and the dielectric confinement give contributions of 0.38 and 0.21 meV, respectively, to the hh-e exciton binding energy close to its maximum value (E_b

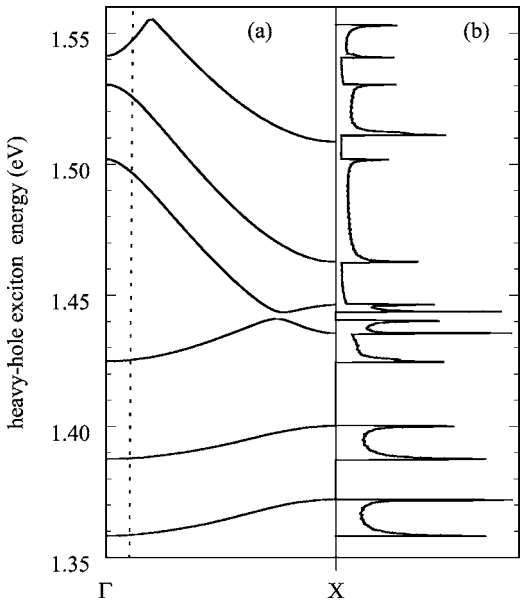

FIG. 5. Energy bands (a) and density of states (b), computed for the hh-e in $In_xGa_{1-x}As/GaAs(001)$ SLQW: well thickness, 5 nm; barrier thickness, 8 nm.

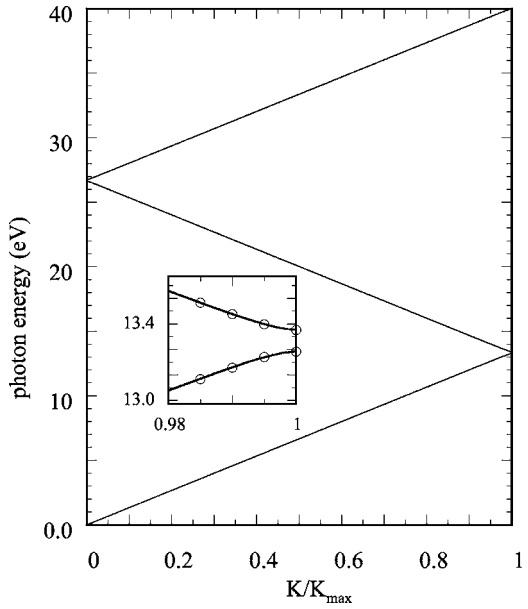

FIG. 7. Computed photonic dispersion curves. In the inset: an enlarged view of the first photonic gap (full lines) is compared with the first polariton gap (circles).

=5.57 meV). While contributions as large as 0.47 and 0.19 meV, respectively, are observed in the case of light-hole binding energy maximum value (E_b=4.19 meV). Finally, the computed exciton binding energies reach the bulk limit values of GaAs for very thin and of $In_xGa_{1-x}As$ for very thick well widths.

The binding energy trend, as a function of the well width, is usually described as due to the squeezing that the confinement produces on the Wannier exciton. This allows us to describe the dynamics of the quantum-confined exciton as a hybrid between two-dimensional and three-dimensional exciton behaviors. As a consequence, excitons can be thought to move in a space whose dimension can assume all the values between 2 and 3. This dimensional behavior of excitons in confined systems can be described by using the so-called fractional-dimensional space.

The use of the fractional-dimensional space was introduced by He[36] in order to describe the dynamics of systems that are supposed to move in a space with no integer dimension, as Wannier excitons in quantum-confining systems. In this approach the anisotropy produced by the confining potential in a three-dimensional space is reduced to an isotropic problem but in a fractional-dimensional space, whose dimension D_f depends on the degree of anisotropy[37] produced by

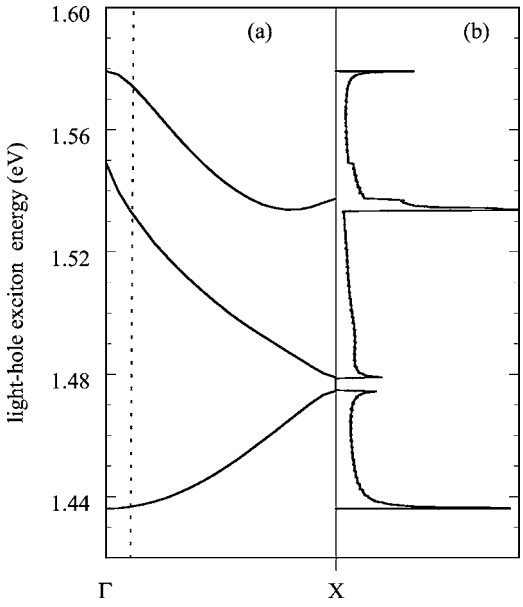

FIG. 6. Energy bands (a) and density of states (b), computed for the lh-e in an $In_xGa_{1-x}As/GaAs(001)$ SLQW: well thickness, 5 nm; barrier thickness, 8 nm.

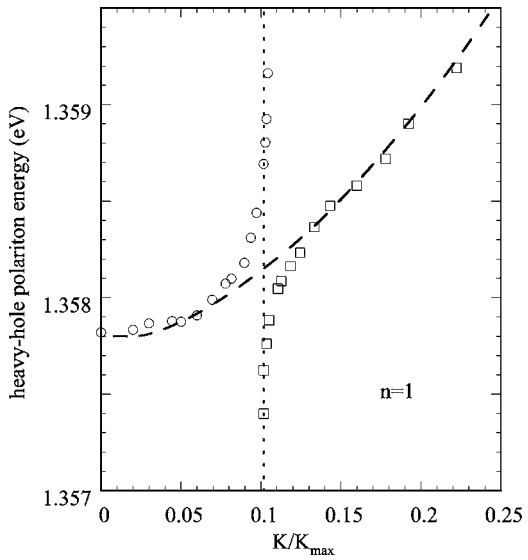

FIG. 8. Upper (circles) and lower (squares) polaritonic energy branches, computed for the first hh-e state (n=1) in $In_xGa_{1-x}As/GaAs(001)$ SLQW. Bare exciton and photon dispersion curves are also reported.

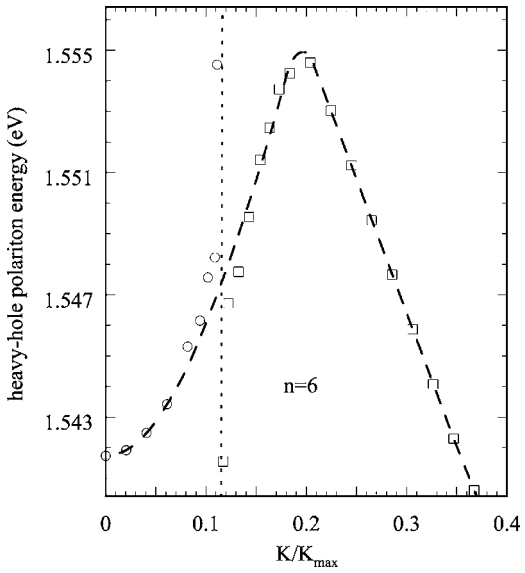

FIG. 9. Upper (circles) and lower (squares) polaritonic energy branches, computed for the sixth hh-e state ($n=6$) in $In_xGa_{1-x}As/GaAs(001)$ SLQW. Bare exciton and photon dispersion curves are also reported.

the geometry of the confinement, namely, well width, barrier height, image potential, and mass ratio.

For Wannier excitons in the fractional-dimensional space, the formal solution of the Schrödinger equation, performed by using the Laplacian operator proposed by Stillinger,[38] gives, for the first state of the exciton binding energy, the following scaling equation:

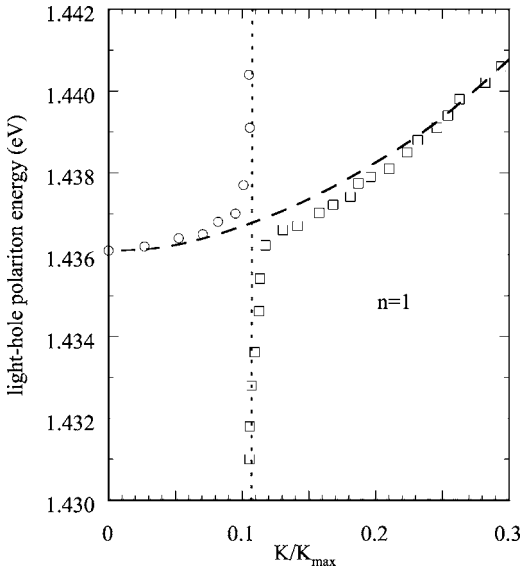

FIG. 10. Upper (circles) and lower (squares) polaritonic energy branches, computed for the first lh-e state ($n=1$) in $In_xGa_{1-x}As/GaAs(001)$ SLQW. Bare exciton and photon dispersion curves are also reported.

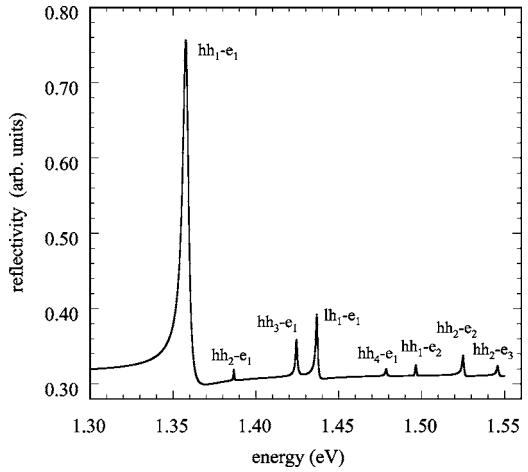

FIG. 11. Normal incidence reflectivity of $In_xGa_{1-x}As/GaAs(001)$ SLQW.

$$E_b(D_f) = \frac{4}{(D_f-1)^2} E_b(3D), \tag{26}$$

where $E_b(3D)$ is the binding energy of the lowest energy state of the three-dimensional bulk exciton of $Ga_{1-x}In_xAs$ alloy ($E_b=4.36$ meV and $E_b=3.65$ meV, for hh-e and lh-e, respectively), and $E_b(D_f)$ is the corresponding value in the fractional-dimensional space. Now, by using the computed values of binding energy of Fig. 2 for $E_b(D_f)$, we obtain from the former equation the fractional dimension of Wannier exciton confined in SLQW. This result is shown in Fig. 4. It should be noticed that, for well widths smaller than 0.5 nm, the exciton is nearly localized in the barriers and, therefore, the $D_f=3$ value can be achieved by using the bulk binding energy of barrier material (GaAs) instead of the well material ($In_xGa_{1-x}As$).

We have computed the exciton energy bands and the exciton density of states for a SLQW with well width $L_w=8$ nm. This value has been chosen in correspondence of the first maximum of the binding energy of the hh-e, where the exciton is very sensitive to the SLQW confinement. The computed dispersion curves are shown in Fig. 5 for hh-e and in Fig. 6 for lh-e, respectively. In the same figures, the photon dispersion curves, obtained from the solutions of Eq. (17) by neglecting the exciton contribution ($S_o=0$), are also shown (dotted line). The lowest energy dispersion curves of hh-e are flatter than the corresponding lh-e curves due to the heavier total mass and to the higher localization in the well region. The Wannier exciton total mass shows different behaviors for higher energy dispersion curves; in fact, close to the Γ point, the $n=6$ heavy exciton state shows a total effective mass lighter than that observed for the lowest light exciton band ($n=1$). Therefore, in this case, very large nonlocal effects should be observed in the optical spectrum. Besides, the effective total mass of hh-e becomes negative in the zones where the dispersion curve changes its slope and the group velocity goes to zero (see Fig. 5); in these zones, analogous to the high symmetry points of the BZ, high density of excitonic states is observed.

The energy dispersion curves, computed for the lh-e, are shown in Fig. 6. Also, in this case, we observe large exciton density of states at high symmetry points of the BZ and where the dispersion curve changes its slope. Finally, the light-hole exciton energy gaps look smaller than the heavy-hole ones and this is essentially due to the lower exciton localization into the wells experienced by this kind of exciton (see Fig. 4).

B. Polaritons in SLQW

The lowest energy photonic dispersion curves, obtained by wiping out in the calculations the photon-exciton interaction, are shown in Fig. 7. All curves look rather linear in this energy scale, and the photonic gaps drop far from the exciton transition energy range. Moreover, we want to emphasize that the exciton-photon interaction does not affect the optical gaps as can be seen in the inset of Fig. 7, where the computed first photonic gap (full line) is shown together with the corresponding polaritonic gap (circles).

The solution of Eq. (17), as a function of the wave vector $\boldsymbol{K}$ values in the first BZ, gives the polariton dispersion curves. The first and the sixth hh-e states ($n=1,6$), and the first lh-e state ($n=1$) are shown in Figs. 8–10, respectively. In the same pictures, the excitonic (dashed line) and photonic (dotted line) bands are also reported for the sake of comparison.

For excitons perfectly confined in a single quantum well, the polaritonic splitting energy decreases by increasing the transition energy; in the present case, we obtain about 1.2 meV for hh-e that has strong probability to be confined in the wells (Fig. 8), while it is about 6.2 meV for light exciton (Fig. 10) and 7.3 meV for $n=6$ heavy exciton state (Fig. 9), which has a high probability to be confined in the barriers. It should be noticed that for the latter exciton state ($n=6$) the rather larger polariton splitting value is due to the high spatial dispersion properties (high penetration in the barriers, low exciton effective mass, etc.). In fact, the spatial dispersion scales as the inverse of the effective total mass and, rather close to the Γ point of the reciprocal lattice, the $n=6$ heavy exciton mass is lower than that of $n=1$ lh-e state. Moreover, for photon energy values far from the radiation-matter interaction range of energy, the computed polaritonic branches quite exactly reproduce the bare exciton or the photon dispersion curves.

The reflectivity spectrum of SLQW at normal incidence, computed by using a well width of 8 nm and nonradiative damping values of $\gamma=0.4$ and $\gamma=0.6$ meV for hh-e and lh-e, respectively, is shown in Fig. 11. In this spectrum, the excitonic transitions are assigned to the couple of electron-hole subband state that gives the major contribution (greater than 80%) to the total excitonic state. All peaks look rather asymmetric and shifted a little with respect to the exciton energy values.

The spatial dispersion removes the symmetry of parity of the SLQW and allows polaritonic states that involve, forbidden for symmetry, odd excitonic states as those corresponding to the peaks labeled hh_2-e_1, hh_4-e_1, and hh_1-e_2 in Fig. 11. Indeed, the oscillator strength of the exciton transition depends on the integral of the exciton wave function and its value is always zero for odd states. Differently, the oscillator strength of the polariton depends on the integral of the product of the exciton wave function by the electrical field. Therefore, due to the asymmetric slope of the latter, the integral does not vanish also for odd exciton states. This property is often observed in experimental optical spectra, but it is mainly attributed to the loss of symmetry due to the disorder of the heterostructure that, instead, is completely missed in our model calculation.

IV. CONCLUSIONS

We have studied the optical response of a SLQW by self-consistent calculations of the Maxwell and Schrödinger equations in the semiclassical framework and in the effective-mass approximation. The confinement properties of heavy and light excitons in SLQW have been studied and compared with analogous results computed in the single quantum well. It has been observed that the behavior of the exciton binding energy highlights different kinds of confinement in the superlattice. Moreover, the results obtained for the different bands emphasize a strong variation of the exciton properties such as (i) exciton effective total mass, (ii) spatial dispersion effect, (iii) exciton optical oscillator strength, and (iv) polariton splitting energy that for suitable values of the physical parameters (alloy compositions, well and barrier widths) could be optimized for the tailoring of the optical properties in semiconductor superlattices.

Finally, the present calculation scheme can be a useful starting point for designing optical devices when an *a priori* knowledge is required of the main effects produced by the confinement properties and polaritonic interactions.

ACKNOWLEDGMENT

The authors are indebted to the Italian project FIRB-MIAO (wp2.2-task 3) of MIUR for financial support.

*Corresponding author. Electronic address: norberto.tomassini@isc.cnr.it

[1] J. B. Xia and B. F. Zhu, *Semiconductor Superlattice Physics* (Shanghai Science and Technology, Shanghai 1995).

[2] D. L. Smith and C. Mailhiot, Rev. Mod. Phys. **62**, 173 (1990).

[3] N. F. Johnson, H. Ehrenreich, P. M. Hui, and P. M. Young, Phys. Rev. B **41**, 3655 (1990).

[4] K. Cho, *Optical Response of Nanostructures Microscopic Nonlocal Theory*, Springer Series in Solid-State Sciences Vol. 139 (Springer, Berlin, 2003).

[5] T. Stroucken, A. Knorr, T. Thomas, and S. W. Koch, Phys. Rev. B **53**, 2026 (1996).

[6] S. Nojima, Phys. Rev. B **59**, 5662 (1999).
[7] S. Fafard, Y. H. Zhang, and J. L. Merz, Phys. Rev. B **48**, 12308 (1993).
[8] N. Tomassini, A. D'Andrea, G. Martino, R. Girlanda, and R. Atanasov, Phys. Rev. B **52**, 11113 (1995).
[9] N. Tomassini, L. Pilozzi, D. Schiumarini, and A. D'Andrea, Recent Res. Dev. Appl. Phys. **6**, 569 (2003).
[10] T. Ikawa and K. Cho, Phys. Rev. B **66**, 085338 (2002).
[11] L. Pilozzi, A. D'Andrea, and K. Cho, Phys. Rev. B **69**, 205311 (2004).
[12] K. J. Moore, G. Duggan, A. Raukema, and K. Woodbridge, Phys. Rev. B **42**, 1326 (1990).
[13] K. J. Moore, G. Duggan, K. Woodbridge, C. Roberts, N. J. Pulsford, and R. J. Nicholas, Phys. Rev. B **42**, 3024 (1990).
[14] F. H. Pollak, Surf. Sci. **37**, 863 (1973).
[15] J. H. Marzin, in *Heterostructures and Semiconductors Superlattices*, edited by G. Allan, G. Bastard, N. Boccara, and M. Voos (Spinger-Verlag, Berlin, 1985).
[16] L. Laude, F. H. Pollak, and M. Cardona, Phys. Rev. B **3**, 2623 (1971).
[17] F. H. Pollak, in *Semiconductors and Semimetals*, edited by T. P. Paersal (Academic, New York 1990), Vol. 32.
[18] R. Atanasov, F. Bassani, A. D'Andrea, and N. Tomassini, Phys. Rev. B **50**, 14381 (1994).
[19] G. Bastard, *Wave Mechanics Applied to Semiconductor Heterostructures* (Les Edition De Physique, Les Ulis, 1988).
[20] H. Haken, *Quantum Field Theory of Solids* (North-Holland, Amsterdam, 1988), p. 211.
[21] L. V. Keldysh, Superlattices Microstruct. **4**, 637 (1966).
[22] B. Gil, P. Lefebvre, P. Boring, K. J. Moore, G. Duggan, and K. Woodbridge, Phys. Rev. B **44**, 1942 (1991).
[23] B. Jogai and P. W. Yu, Phys. Rev. B **41**, 12650 (1990).
[24] J. M. Luttinger and W. Kohn, Phys. Rev. **97**, 869 (1955).
[25] J. M. Luttinger, Phys. Rev. **102**, 1030 (1956).
[26] C. Aldrich and K. K. Bajaj, Solid State Commun. **22**, 157 (1977).
[27] R. Chen and K. K. Bajaj, Phys. Status Solidi B **199**, 417 (1979).
[28] M. Kumagai and T. Takagahara, Phys. Rev. B **40**, 12359 (1989).
[29] D. B. Tran Thoai, R. Zimmermann, M. Grundmann, and D. Bimberg, Phys. Rev. B **42**, 5906 (1990).
[30] *Semiconductors Physics of Group IV Elements and III-V compounds*, Landolt-Bornstein, New Series, Group III, Vol. 17, edited by O. Madelung (Springer, Berlin, 1982), Pt. A.
[31] S. Adachi, J. Appl. Phys. **53**, 8775 (1982).
[32] A. D'Andrea, N. Tomassini, L. Ferrari, M. Righini, S. Selci, M. R. Bruni, D. Schiumarini, and M. G. Simeone, J. Appl. Phys. **83**, 7920 (1998).
[33] A. D'Andrea, N. Tomassini, L. Ferrari, M. Righini, S. Selci, M. R. Bruni, M. G. Simeone, and N. Gambacorti, Phys. Rev. B **52**, 10713 (1995).
[34] A. Baghi, R. G. Barrera, and A. K. Rajagopal, Phys. Rev. B **20**, 4824 (1980).
[35] S. I. Pekar, Sov. Phys. JETP **6**, 785 (1958).
[36] Xing-Fei He, Phys. Rev. B **43**, 2063 (1991).
[37] Xing-Fei He, Solid State Commun. **75**, 111 (1990).
[38] F. H. Stillinger, J. Math. Phys. **18**, 1224 (1977).